The timing of phasic transmitter release is Ca^{2+}-dependent and lacks a direct influence of presynaptic membrane potential

Felix Felmy, Erwin Neher, and Ralf Schneggenburger*

AG Synaptische Dynamik und Modulation and Abteilung Membranbiophysik, Max-Planck-Institut für Biophysikalische Chemie, Am Fassberg 11, D-37077 Göttingen, Germany

Edited by Charles F. Stevens, The Salk Institute for Biological Studies, La Jolla, CA, and approved October 6, 2003 (received for review May 30, 2003)

Ca^{2+} influx through voltage-gated Ca^{2+} channels and the resulting elevation of intracellular Ca^{2+} concentration, $[Ca^{2+}]_i$, triggers transmitter release in nerve terminals. However, it is controversial whether in addition to the opening of Ca^{2+} channels, membrane potential directly affects transmitter release. Here, we assayed the influence of membrane potential on transmitter release at the calyx of Held nerve terminals. Transmitter release was evoked by presynaptic Ca^{2+} uncaging, or by presynaptic Ca^{2+} uncaging paired with presynaptic voltage-clamp depolarizations to +80 mV, under pharmacological block of voltage-gated Ca^{2+} channels. Such a change in membrane potential did not alter the Ca^{2+} dependence of transmitter release rates or synaptic delays. We also found, by varying the amount of Ca^{2+} influx during Ca^{2+} tail-currents, that the time course of phasic transmitter release is not invariant to changes in release probability. Rather, the time difference between peak Ca^{2+} current and peak transmitter release became progressively shorter with increasing Ca^{2+} current amplitude. When this time difference was plotted as a function of the estimated local $[Ca^{2+}]_i$ at the sites of vesicle fusion, a slope of $\approx$100 μs per 10 μM $[Ca^{2+}]_i$ was found, in reasonable agreement with a model of cooperative Ca^{2+} binding and vesicle fusion. Thus, the amplitude and time course of the $[Ca^{2+}]_i$ signal at the sites of vesicle fusion controls the timing and the amount of transmitter release, both under conditions of brief periods of Ca^{2+} influx, as well as during step-like elevations of $[Ca^{2+}]_i$ produced by Ca^{2+} uncaging.

Transmitter release occurs when an action potential (AP) invades the presynaptic nerve terminal and opens voltage-gated Ca^{2+} channels, allowing a brief influx of Ca^{2+} ions into the presynaptic terminal (1–5). It is thought that the brief increase in release probability underlying phasic transmitter release (6) is caused by the transient increase in local $[Ca^{2+}]_i$ (intracellular free Ca^{2+} concentration) at the sites of vesicle fusion, resulting from this AP-induced Ca^{2+} influx. The local $[Ca^{2+}]_i$ signal for vesicle fusion arises from Ca^{2+} microdomains (7, 8) formed by individual Ca^{2+} channels (9), or, alternatively, from the overlap of Ca^{2+} microdomains created by several neighboring Ca^{2+} channels (4, 10). We previously inferred the amplitude and the time course of the local $[Ca^{2+}]_i$ signal seen by readily releasable vesicles, on the basis of the intracellular Ca^{2+} sensitivity of transmitter release determined by Ca^{2+} uncaging (ref. 11; see also refs. 12–14). This back-calculation, however, assumes that the local $[Ca^{2+}]_i$ at the sites of vesicle fusion is the only determinant of transmitter release probability on a short timescale.

It is controversial whether factors other than the time course of local $[Ca^{2+}]_i$ influence the timing and the amount of phasic release. At the neuromuscular junction, it has been shown that a strong reduction of release probability, imposed by reducing the amount of Ca^{2+} influx, does not change the time course of phasic release during a presynaptic AP (15–17). It has been proposed that this invariance of the time course of transmitter release against changes in Ca^{2+} influx implies that additional factors, other than the rapid rise and fall of the $[Ca^{2+}]_i$ at the sites of vesicle fusion, must be involved in controlling the time course of phasic release (18). This additional factor was suggested to be a direct effect of presynaptic membrane potential on transmitter release (refs. 16, 18, and 19; but see also refs. 20–22). More recently, effects of membrane potential on transmitter release received renewed attention when Zhang and Zhou (23) described Ca^{2+}-independent but voltage-dependent vesicle fusion from dorsal root ganglion cells. Mechanisms for the coupling of membrane potential to the release apparatus were suggested to involve the voltage sensor of N-type Ca^{2+} channels (24). Alternatively, voltage-sensitive binding of acetylcholine to presynaptic muscarinic receptors was proposed to directly influence the release machinery via protein–protein interactions (25).

Here, we use paired pre- and postsynaptic whole-cell voltage-clamp recordings at the calyx of Held, combined with Ca^{2+} uncaging in the presynaptic nerve terminal, to address the question whether presynaptic membrane potential has a direct effect on transmitter release.

Materials and Methods

Electrophysiology, Slice Preparation, and Solutions. Transverse brainstem slices containing the medial nucleus of the trapezoid body (MNTB) were made, by using 8- to 10-day-old Wistar rats. We made simultaneous pre- and postsynaptic whole-cell recordings at room temperature (21–24°C) from the calyx of Held to MNTB principal cell synapse with an EPC-9 double patch clamp amplifier (HEKA Electronics, Lambrecht, Germany). Cells were visualized in an upright microscope (Zeiss, Oberkochen, Germany) equipped with gradient contrast, infrared illumination (Luigs and Neumann, Ratingen, Germany). The extracellular recording solution contained (in mM) 125 NaCl, 25 $NaHCO_3$, 2.5 KCl, 1.25 NaH_2PO_4, 1 $MgCl_2$, 1 $CaCl_2$, 25 glucose, 0.4 ascorbic acid, 3 myo-inositol, and 2 sodium-pyruvate; and 10 mM tetraethylammoniumchloride (TEA-Cl), 50 μM D-(−)-2-amino-5-phosphonopentanoic acid, 0.5 μM tetrodotoxin, 100 μM cyclothiazide. The pH of the recording solution was 7.4 when bubbled with 95% O_2 and 5% CO_2. For the experiments of Fig. 4, the extracellular solution contained 4 mM $CaCl_2$ and 1 mM kynurenic acid, and 0.1 mM 3.4-diaminopyridine were added. For the experiments in Figs. 1–3, Ca^{2+} currents were suppressed with 200 nM ω-agatoxin (Peptide Institute, Osaka) and 1 μM ω-conotoxin GVIA (Tocris, Bristol, U.K.). Cytochrome *c* (0.1 mg/ml; Sigma) was always present in toxin-containing solutions (26, 27). The pipette solution for postsynaptic recordings always contained (in mM): 130 cesium-gluconate, 10 Cs-Hepes, 20 TEA-Cl, 4 MgATP, 0.3 Na_2GTP, and 5 Cs_2-EGTA. For the experiments shown in Figs. 4 and 5, the pipette solution for

This paper was submitted directly (Track II) to the PNAS office.

Abbreviations: AP, action potential; EPSC, excitatory postsynaptic current; $[Ca^{2+}]_i$, intracellular free Ca^{2+} concentration.

*To whom correspondence should be addressed. E-mail: rschneg@gwdg.de.

www.pnas.org/cgi/doi/10.1073/pnas.2433276100

presynaptic recordings contained (in mM): 130 cesium-gluconate, 10 Cs-Hepes, 20 TEA-Cl, 3.3 $MgCl_2$, 2 Na_2ATP, and 0.3 Na_2GTP.

Ca^{2+} Uncaging and Ca^{2+} Imaging. For the Ca^{2+} uncaging experiments (Figs. 1 and 2), the presynaptic pipette solution contained (in mM): 120 cesium-gluconate, 20 Cs-Hepes, 20 TEA-Cl, 5 Na_2ATP, 0.3 Na_2GTP, 1.5 DM-nitrophen, 1.2 $CaCl_2$, 0.8 $MgCl_2$, and 100 μM fura-2FF as Ca^{2+} indicator. A flash lamp (Rapp Optoelektronik, Hamburg, Germany) was used to photolyze DM-nitrophen. $[Ca^{2+}]_i$ was measured by exciting fura-2FF (350/380 nm) with a monochromator and imaging the resulting fluorescence with a charge-coupled device camera (TILL Photonics, Gräfelfing, Germany). Pixel binning was 8×15, allowing short (5-ms) exposure times for each image. $[Ca^{2+}]_i$ was calculated from background-corrected fluorescence ratios with the equation derived in ref. 28. The calibration of fura-2FF for the Ca^{2+} uncaging experiments was as described in ref. 14.

EPSC Deconvolution and Data Analysis. Transmitter release rates were extracted by deconvolving excitatory postsynaptic current (EPSCs) (29). For the deconvolution, we assumed that the average miniature EPSC (mEPSC) amplitude was 30 pA in each cell, a value that closely matches the mean of mEPSC amplitudes recorded in this preparation at a similar developmental stage (30, 31). In the presence of 1 mM kynurenic acid (Fig. 4), the mean mEPSC amplitude was assumed to be reduced by 50% (31).

For fitting the data in Fig. 3 *a* and *c*, we first calculated numerically the expected rise in $[Ca^{2+}]_i$ after a flash using the measured time course of the flash-lamp (1.1-ms half-width) and the kinetics of the involved Ca^{2+} and Mg^{2+} buffers. The resulting Ca^{2+} waveform had a 10–90% rise time of 0.95 ms, and did not decay >5% in the first 10 ms after its peak. This $[Ca^{2+}]_i$ waveform was used to drive a kinetic model (11, 14) that assumes that 5 Ca^{2+} ions bind cooperatively to the Ca^{2+} sensor for vesicle fusion before an irreversible fusion step. By fitting the control data (Fig. 3 *a* and *b*) using a fixed cooperativity factor $b = 0.25$, we obtained the following parameters: $k_{on} = 1.19 \times 10^8\ M^{-1} \cdot s^{-1}$, $k_{off} = 8{,}745\ s^{-1}$, and fusion rate $\gamma = 6{,}995\ s^{-1}$. For this fit, we assumed that the number of readily releasable vesicles was the same as determined previously with pool-depleting voltage-clamp steps (1,800 on average; see figure 3 of ref. 14). This assumption was necessary because in the experiments shown in Figs. 1–3, the pool size could not be estimated by voltage-clamp steps, due to the presence of Ca^{2+} channel blockers. Delays of flash responses (Fig. 3*b*) are given as the time between the trigger for the flash lamp, and the time at which 3 quanta were released in integrated release rate traces.

Compensation of Voltage-Clamp Errors. For the experiments shown in Figs. 4 and 5, filtering effects caused by voltage-clamp errors had to be prevented or otherwise compensated off-line. We attempted to minimize the series resistances R_s in simultaneous pre- and postsynaptic recordings (ranges, 12–20 MOhm and 4–8 MOhm, respectively). During recordings, the cell capacitance cancellation circuit of the EPC-9 was active, and R_s was electronically compensated by 50–80% (presynaptic recordings) and by 80–90% (postsynaptic recordings). Currents were low-pass filtered at 8 kHz with the built-in Bessel filter of the EPC-9 before sampling at 50 kHz.

Presynaptic currents were corrected off-line for capacitative and leak currents with a standard P/5 protocol. The resulting current traces (see Fig. 4*a*, dotted traces), however, do not faithfully reflect the membrane Ca^{2+} current because of a mismatch of the true capacitative current (I_{cap}) during the voltage-clamp step from +100 to −80 mV, and the estimate of the capacitative current (I_{cap}') made by the capacitance cancellation circuit together with the P/5 protocol. This mismatch arises because the cancellation circuit and the P/5 protocol assume (or measure) an exponential charging time constant whereas the Ca^{2+} currents during repolarization lead to deviations from this ideal case. This error was corrected according to a one-compartment electrotonic model of the cell (32). First, I_{cap}' was calculated by using the resting value of membrane resistance R_m and membrane capacitance C_m, and the fraction of R_s remaining after electronic compensation (R_s'). The calculated I_{cap}' was added to the P/5 corrected trace, giving I_{tot}' (the estimated sum of capacitative and resistive current in the absence of capacitance cancellation and P/5 correction). Second, I_{tot}' and R_s' were used to calculate the time course of membrane potential V_m during the step from +100 to −80 mV, and the correct capacitative current, I_{cap}, was calculated from C_m and the time-derivative of V_m. Finally, I_{cap} was subtracted from I_{tot}', giving an estimate of the correct ionic current during the step from +100 to −80 mV (Fig. 4*a*, solid traces). This correction preserved the total charge flowing upon repolarization but increased the amplitudes and decreased the half-widths of the current traces. Postsynaptic currents were corrected off-line by standard procedures for R_s errors (30) (compare dotted and solid traces in Fig. 4*B*).

Estimate of the local $[Ca^{2+}]_i$ and Predictions of Transmitter Release. For each repolarization-evoked EPSC (Fig. 4), we estimated the local $[Ca^{2+}]_i$ signal for phasic release compatible with the Ca^{2+} sensitivity determined in the experiments of Figs. 1–3. For this analysis, the corresponding Ca^{2+}-tail current after off-line correction (Fig. 4*a*, solid traces) was used as a template $[Ca^{2+}]_i$ waveform. The current waveforms were inverted and normalized and were then used to drive a model of cooperative Ca^{2+} binding and vesicle fusion (11), with the model parameters obtained from the fit in Figs. 3 *a* and *b*. The amplitude of the $[Ca^{2+}]_i$ waveform was varied until the time-course and amplitude of the predicted transmitter release rate matched the measured release rate. In this approach, the timing between Ca^{2+} current and transmitter release was left unchanged. The pool sizes in these experiments (range 1,540–4,420 quanta; average 2,400) were estimated by presynaptic depolarizations of 50 ms to 0 mV, which caused large Ca^{2+} currents and rapidly depleted the readily releasable pool (see, e.g., figure 3 in ref. 14). For the model predictions in Fig. 5*b*, the average pool size was used together with a selected Ca^{2+} tail-current.

Results

To investigate whether presynaptic membrane potential has a direct influence on transmitter release, we performed double whole-cell voltage-clamp recordings from calyx of Held terminals and medial nucleus of the trapezoid body principal neurons. In a first series of experiments (Figs. 1 and 2), we induced transmitter release by presynaptic Ca^{2+} uncaging, or by Ca^{2+} uncaging combined with presynaptic voltage-clamp depolarizations to +80 mV. To minimize Ca^{2+} entry through voltage-gated Ca^{2+} channels during the depolarizations, ω-agatoxin (200 nM) and ω-conotoxin (1 μM) were included in the extracellular recording solution to block N- and P/Q-type channels (26, 27), and the extracellular $[Ca^{2+}]$ was reduced to 1 mM.

In the experiment shown in Fig. 1, a control flash, a flash paired with presynaptic depolarization, and another control flash were applied sequentially, at intervals of >1 min. The resulting elevations in $[Ca^{2+}]_i$ were similar for the three stimuli (range, 3.3 to 3.9 μM). The EPSC evoked by the combined stimulus of Ca^{2+} uncaging and presynaptic depolarization (black trace in Fig. 1*b*) was similar to the control EPSCs (gray traces in Fig. 1*b*), and no acceleration of the EPSC was obtained at the instant of membrane depolarization (Fig. 1*b*, arrow). The EPSCs were deconvolved (29) to obtain transmitter release rates (Fig.

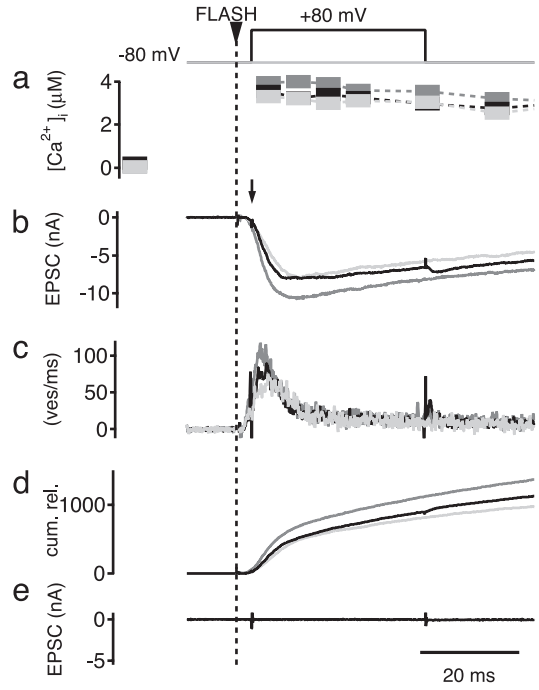

Fig. 1. Presynaptic membrane depolarization does not enhance transmitter release triggered by Ca^{2+} uncaging. (*a–d*) Presynaptic $[Ca^{2+}]_i$ elevations by flash-induced Ca^{2+} uncaging (*a*), postsynaptic membrane current (*b*), transmitter release rates derived by deconvolution analysis (*c*), and the integrated transmitter release rates (*d*). Traces are from a first control flash (light gray traces), from a second flash that was paired with a 34-ms depolarization to +80 mV (black traces), and from a subsequent control flash (dark gray traces). Note that, at the instant of presynaptic depolarization, no acceleration of the EPSC was apparent (see black trace and vertical arrow in *b*). In *e*, the postsynaptic current response to a depolarization applied without Ca^{2+} uncaging is shown. The vertical dotted line indicates the time at which the flash was given.

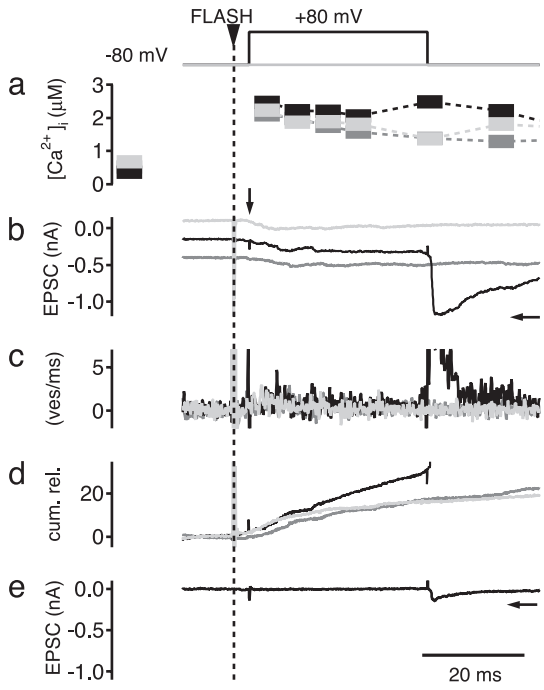

Fig. 2. Presynaptic membrane depolarization does not enhance low rates of Ca^{2+}-dependent transmitter release. Shown is an experiment similar to that shown in Fig. 1, but using attenuated flashes that elevated the presynaptic $[Ca^{2+}]_i$ to 2.1–2.4 μM (*a*), evoking slowly rising small EPSCs (*b*) indicative of low rates of transmitter release (*c*). The grayscale code of the traces is as in Fig. 1. The traces in *b* were vertically offset for better visibility. Note that a small EPSC was triggered on repolarization in the absence of Ca^{2+} uncaging (*e*, horizontal arrow). This tail-evoked EPSC was enhanced 5.8-fold in amplitude when an identical depolarization was paired with Ca^{2+} uncaging (*b*, horizontal arrow).

1*c*). The control peak transmitter release rates were 60 ves/ms and 107 ves/ms, flanking the test trial of 79 ves/ms (Fig. 1*c*). Thus, there was a trend toward larger release rates, which correlated with a similar trend toward larger postflash $[Ca^{2+}]_i$ elevations in this experiment (compare light gray, black, and dark gray traces in Fig. 1 *c* and *a*). However, there was no effect of presynaptic membrane depolarization on transmitter release evoked by Ca^{2+} uncaging.

We next tested whether transmitter release at lower presynaptic $[Ca^{2+}]_i$ might be more sensitive to a direct effect of presynaptic membrane potential. Fig. 2 shows an experiment in which flashes elevated $[Ca^{2+}]_i$ to 2.1–2.4 μM and evoked slowly rising EPSCs with amplitudes of ≈150 pA, indicative of more asynchronous transmitter release (Fig. 2 *a–c*). The EPSC and the transmitter release rates derived from the EPSCs were unchanged within the first 15 ms after the onset of presynaptic membrane depolarization. Because a proposed positive effect of membrane depolarization on transmitter release should occur within a few milliseconds or less (18, 33, 34), release rates and cumulative release should be accelerated directly after the depolarization (Fig. 2*b*, vertical arrow), which was not observed. The sustained increase in the cumulative release rates during the last part of the depolarization (Fig. 2*d*, black trace) is likely due to accumulation of $[Ca^{2+}]_i$ late during depolarizations. Such a Ca^{2+} accumulation might be caused by incomplete Ca^{2+} channel block by ω-agatoxin and ω-conotoxin and/or by Ca^{2+} influx through R-type channels (26, 27), which adds to the $[Ca^{2+}]_i$ elevations induced by the flash.

In the example shown in Fig. 2*b*, the combined stimulus of Ca^{2+} uncaging and presynaptic depolarization caused a rapidly rising EPSC on repolarization (Fig. 2*b*, black trace, horizontal arrow). This response was mediated by a small remaining Ca^{2+} tail current (not shown), which caused an EPSC that was further facilitated by presynaptic Ca^{2+} uncaging (14). Indeed, when the same presynaptic depolarization was applied without Ca^{2+} uncaging, a much smaller EPSC was evoked (Fig. 2*e*, horizontal arrow). The degree of facilitation in this example (5.8-fold; compare repolarization-evoked EPSCs in Fig. 4 *e* and *b*), induced by a flash-evoked $[Ca^{2+}]_i$ elevation to ≈2 μM, agrees well with the intracellular Ca^{2+} sensitivity of facilitation observed previously (14). Thus, incomplete block of Ca^{2+} channels by the toxins, combined with facilitation of transmitter release, can account for the repolarization-evoked EPSCs.

Fig. 3 shows a summary of the experiments aimed at testing the effect of presynaptic membrane depolarization on the Ca^{2+}-dependent properties of transmitter release. Peak transmitter release rates (Fig. 3*a*), delay times for transmitter release (Fig. 3*b*), and the time to peak of transmitter release (Fig. 3*c*) were plotted as a function of $[Ca^{2+}]_i$ attained after UV flashes (n = 11 paired recordings). For all measured parameters, the control flashes (Fig. 3, open symbols) overlapped with the trials in which Ca^{2+} uncaging was paired with membrane depolarization (Fig. 3, filled symbols). Fitting the Ca^{2+} dependence of peak transmitter release rates and the delays with a model of cooperative Ca^{2+} binding and vesicle fusion gave the following parameters: $k_{on} = 1.19 \times 10^8\ M^{-1}{\cdot}s^{-1}$, $k_{off} = 8745\ s^{-1}$ and a fusion rate of $\gamma = 6995\ s^{-1}$ (Fig. 3 *a* and *b* and *Materials and Methods*). These values are similar to the ones of previous studies (11, 14). To see whether a change occurred between the control and test con-

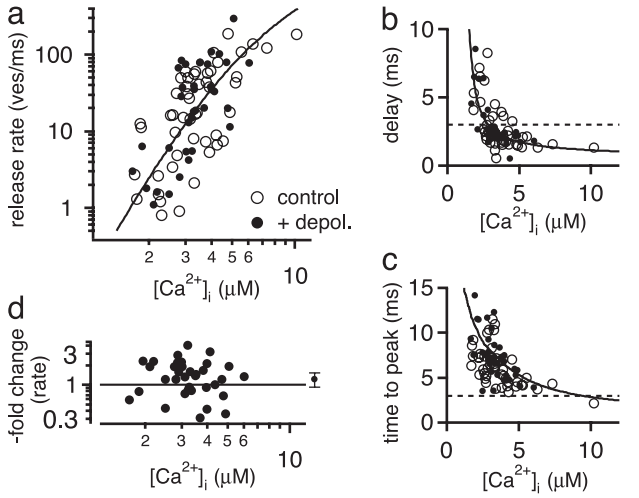

Fig. 3. The intracellular Ca^{2+} dependence of transmitter release rates and release kinetics are not affected by presynaptic membrane depolarization. (*a–c*) Peak transmitter release rates (*a*), synaptic delays (*b*), and the time to peak transmitter release (*c*) are plotted as a function of the presynaptic $[Ca^{2+}]_i$ attained after flashes. Data from $n = 11$ paired recordings from Figs. 1 and 2 are shown. Open and filled symbols represent data from control flashes, and from flashes paired with presynaptic depolarizations to +80 mV, respectively. The solid lines indicate the fit of a model of cooperative binding of five Ca^{2+} ions, followed by an irreversible fusion step (11). The model parameters of this fit are given in *Materials and Methods*. The dotted lines in *b* and *c* indicate the time at which the depolarization was applied (at 3 ms after the flash; see Figs. 1 and 2). (*d*) Plot of the relative change induced by presynaptic depolarization in the peak transmitter release rates ($n = 36$ trials in 11 paired recordings). For this analysis, the fit line shown in *a* was shifted on the *x* axis to minimize the difference to the control data points in each cell. Then, the relative change between the data points was obtained with depolarization, and the corresponding value of the fit line was analyzed. The mean ± SEM of the relative change is shown by the rightmost data point (small symbol with error bars; 1.2 ± 0.3-fold change).

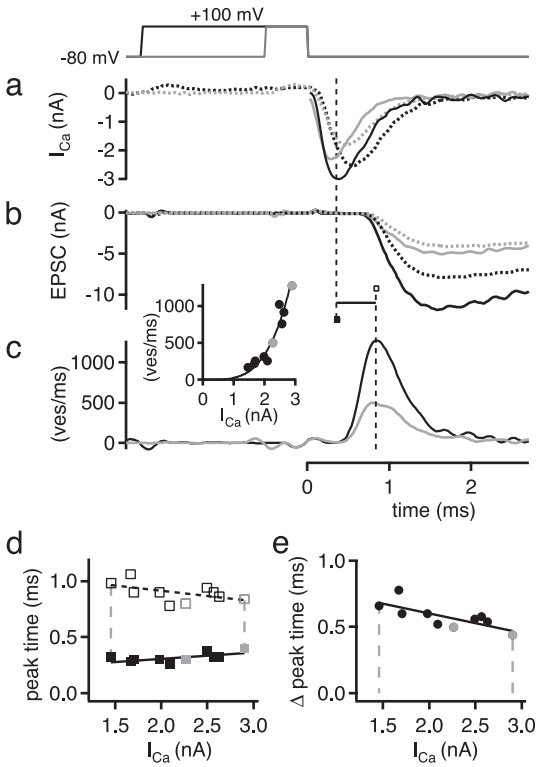

Fig. 4. The time difference between presynaptic Ca^{2+} currents and peak transmitter release depends on the amount of Ca^{2+} influx. (*a–c*) Presynaptic Ca^{2+} current (*a*), postsynaptic membrane current (*b*), and transmitter release rates (*c*) from an experiment in which the duration of a presynaptic depolarization to +100 mV was changed, aimed at evoking Ca^{2+} currents with different amplitudes. Gray and black traces indicate pulse lengths of 0.5 and 2 ms, respectively. The dotted and solid traces in *a* are Ca^{2+}-tail currents after P/5 correction, and after additional off-line correction of a voltage-clamp error, respectively (see *Materials and Methods*). The dotted and solid traces in *b* are measured EPSCs, and EPSCs after off-line correction of the estimated R_s error (30). The *Inset* in *c* shows a plot of the peak release rates as a function of the peak Ca^{2+} currents, fitted with a power function with exponent of $n = 3.8$. (*d*) The peak time of Ca^{2+} currents (filled squares) and transmitter release rates as a function of Ca^{2+} current amplitudes. Each data set was fitted by linear regression, with slopes of −50 μs/nA and 100 μs/nA for release rates (open squares) and Ca^{2+} currents (filled squares), respectively. (*e*) The peak time difference between Ca^{2+} currents and release rates was calculated as the difference of the data sets shown in *d*, and fitted by linear regression (slope, −147 μs/nA). Data throughout are from the same paired recording.

ditions, we compared the transmitter release rates for a given cell pair. The control values for a given terminal were fitted with a model of cooperative Ca^{2+} binding and vesicle fusion. The deviation between this fit line and the data points from flashes paired with depolarizations was analyzed for each cell and plotted as a function of postflash $[Ca^{2+}]_i$ (Fig. 3*d*; see legend to Fig. 3 for details). The resulting data points indicate the relative change in transmitter release rates on presynaptic depolarization to +80 mV and scattered around unity. On average, a slight increase in transmitter release rates of 1.2 ± 0.3-fold (mean ± SEM) was found for flashes paired with presynaptic depolarizations.

So far we, have shown that strong presynaptic membrane depolarizations from −80 mV to +80 mV hardly influence the Ca^{2+} sensitivity of transmitter release, nor do they change the Ca^{2+} dependent kinetics of transmitter release (Fig. 3). This finding is compatible with models in which Ca^{2+} binding to the Ca^{2+} sensor for vesicle fusion determines the rate and the kinetics of transmitter release, independent of changes in membrane potential.

We next asked whether the invariance of the transmitter release time course against changes in the magnitude of Ca^{2+} influx, which was previously observed at the neuromuscular junction (15–17), holds at the calyx of Held. This question is relevant because this finding was one of the major reasons for postulating a direct role of membrane potential on transmitter release (18). We made pre- and postsynaptic whole-cell voltage-clamp recordings, in which we evoked presynaptic Ca^{2+} tail-currents by stepping the membrane potential from –80 mV to +100 mV and back (Fig. 4*a*). Changing the duration of these depolarizations allowed us to alter the amplitude of the Ca^{2+} tail-currents without a major change in their time course. This experimental protocol allowed us to verify whether different amounts of Ca^{2+} influx will lead to different timing of transmitter release.

In the experiment shown in Fig. 4, presynaptic depolarizations for 0.5 ms and 2 ms induced Ca^{2+} tail-currents with peak amplitudes of 2.2 nA and 2.9 nA (Fig. 4*a*, solid traces). The resulting EPSCs had amplitudes of 4.9 nA and 11.6 nA, respectively (Fig. 4*b*), and the peak release rates were 499 ves/ms and 1,278 ves/ms (Fig. 4*c*). By varying the duration of the depolarization, we could evoke transmitter release over a wide range of release probabilities (peak release rates of 165 ves/ms up to ≈1,300 ves/ms in this cell). The relationship between peak transmitter release rate and presynaptic Ca^{2+} current amplitude was consistent with a power function with exponent of 3.8 (Fig. 4*c Inset*).

We subsequently analyzed the time of peak Ca^{2+} currents and peak transmitter release (Fig. 4*d*). The peak of the Ca^{2+} current

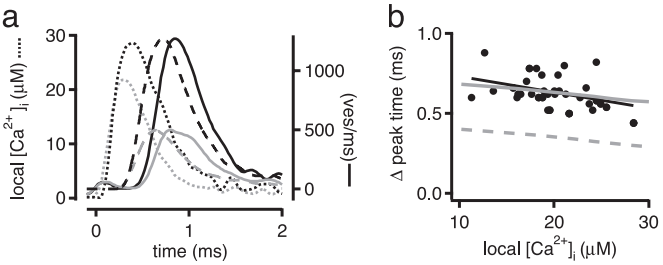

Fig. 5. The observed decrease in peak time difference with increasing $[Ca^{2+}]_i$ is compatible with a simple model of Ca^{2+}-dependent activation of vesicle fusion. (*a*) $[Ca^{2+}]_i$ waveforms (dotted traces), predicted transmitter release rates (broken traces), and measured release rates (solid traces). The $[Ca^{2+}]_i$ waveforms were generated by normalization and appropriate scaling of the Ca^{2+} currents shown in Fig. 4*a* (solid traces; see *Material and Methods* for details). Note that the predicted transmitter release rates are ≈200 μs earlier than the measured ones (same cell as in Fig. 4). (*b*) Plot of peak time difference as analyzed in Fig. 4, as a function of the peak local $[Ca^{2+}]_i$ inferred as shown in *a* for $n = 4$ cells. The data were fitted by linear regression (solid black line), with a slope of −100 μs/μM. The broken gray lines show the predictions of a model of cooperative Ca^{2+} binding and vesicle fusion. This prediction was additionally shifted by 280 μs (solid gray line).

was slightly delayed with increasing Ca^{2+} current amplitudes, with a slope of 100 μs/nA in the example of Fig. 4*d* (filled squares). On the other hand, the peak time of transmitter release rates was progressively earlier with increasing presynaptic Ca^{2+} current amplitudes, with a slope of −50 μs/nA (Fig. 4*d*, open squares). Thus, when the time *difference* between the peak of the Ca^{2+} current and the peak of the transmitter release rate was plotted as a function of Ca^{2+} current amplitude, a slope of −147 μs/nA was found (Fig. 4*e*). Thus, at the calyx of Held, the timing of phasic transmitter release is not invariant against changes in the amount of Ca^{2+} influx. However, it should be noted that the relative decrease of the peak time difference of 31% (Fig. 4*e*) is small compared with the ≈800% increase in peak transmitter release rate (Fig. 4*c Inset*) observed over the same range of Ca^{2+} current amplitudes (1.4–2.9 nA in this cell).

To analyze whether this decrease in the peak time difference with increasing Ca^{2+} influx is compatible with our model of cooperative Ca^{2+} binding and vesicle fusion, we first estimated the local $[Ca^{2+}]_i$ signal which might be seen by an average readily releasable vesicle during Ca^{2+} tail-currents (Fig. 5*a*). For this purpose, we used the normalized and inverted Ca^{2+} current as a first approximation of the $[Ca^{2+}]_i$ waveform. A scaled version of this waveform was used to drive the model of cooperative Ca^{2+} binding and vesicle fusion, with the model parameters as obtained from the fit in Fig. 3 (see *Materials and Methods* for further details). We found that waveforms of local $[Ca^{2+}]_i$ signals with the time course of the Ca^{2+} tail-currents and appropriately scaled amplitudes (Fig. 5*a*, dotted traces) predicted release rate time courses similar to the measured ones (Fig. 5*a*, broken traces), with the only exception that the predicted transmitter release rates were ≈200 μs earlier than the measured release rates (Fig. 5*a*, compare broken and solid lines). This difference is probably caused by the fact that the model of cooperative Ca^{2+} binding and vesicle fusion (11, 14) does not specify events that follow Ca^{2+} binding to the Ca^{2+} sensor of vesicle fusion, such as conformational changes associated with fusion pore opening, diffusion of transmitter out of the vesicle and over the synaptic cleft, and activation of postsynaptic AMPA-receptors. In addition, the cytoplasmic diffusion of Ca^{2+} between the Ca^{2+} channels and the Ca^{2+} sensor for vesicle fusion, which we estimate to be ≈50 μs, is not represented in the model.

The relationship of the peak time differences of Ca^{2+} currents and transmitter release rates is plotted as a function of the estimated local $[Ca^{2+}]_i$ at the sites of vesicle fusion (Fig. 5*b*). The data were fitted with a line, showing a slope of −100 μs/10 μM $[Ca^{2+}]_i$ (Fig. 5*b*, black line). The prediction of the model of cooperative Ca^{2+} binding and vesicle fusion is shown as the broken gray line in Fig. 5*b*. Although the *absolute* peak time difference is smaller than the measured one (see above), the predicted peak time difference also decreases with increasing $[Ca^{2+}]_i$. To enable a direct comparison with the data, the predicted peak time difference is shifted upwards by 280 μs (the unexplained delay; see *Discussion*). The observed slope in the plot of peak time difference vs. local $[Ca^{2+}]_i$ is somewhat larger (100 μs/10 μM $[Ca^{2+}]_i$) than the prediction (56 μs/10 μM $[Ca^{2+}]_i$; see gray line in Fig. 5*b*), although the scatter in the data points is quite large. We conclude that the time difference between the peak of the presynaptic Ca^{2+} currents, and the peak of the transmitter release rates is slightly smaller for larger presynaptic Ca^{2+} influx (Fig. 4*e*). The amount of this peak time difference is compatible with a simple model of Ca^{2+}-dependent activation of vesicle fusion (Fig. 5*b*).

Discussion

We evoked transmitter release at the large calyx of Held synapses by presynaptic Ca^{2+} uncaging or by presynaptic Ca^{2+} uncaging combined with presynaptic depolarizations (Figs. 1 and 2), to assay a proposed direct effect of presynaptic membrane potential on transmitter release (18). A direct effect of membrane depolarization on the Ca^{2+}-dependent parameters of transmitter release, such as peak release rates, and synaptic delay and time to peak transmitter release, was not observed (Fig. 3). The effect of membrane potential proposed in previous work (18) is suggested to be rather instantaneous. Therefore, if voltage had such an effect at the calyx of Held, then we should have observed an acceleration of transmitter release just after the onset of depolarization, which we never did (Figs. 1 and 2, vertical arrows). Hyperpolarization of the nerve terminal was previously found to reduce transmitter release at the neuromuscular junction and therefore was held to contribute to the termination of phasic transmitter release (33, 34). In contrast, we found that hyperpolarization sometimes caused small EPSCs despite the presence of Ca^{2+} channel blockers (Fig. 2*e*). These EPSCs were strongly facilitated when presynaptic $[Ca^{2+}]_i$ was elevated by Ca^{2+} uncaging (compare Fig. 2 *b* and *e*, horizontal arrows), in quantitative agreement with previous work (14). The hyperpolarization-evoked EPSC was caused by a Ca^{2+} tail-current that remained in the presence of the N- and P/Q-type Ca^{2+} channel blockers, indicating incomplete block by the toxins and/or the presence of toxin-insensitive R-type channels (26). In additional experiments, in which all Ca^{2+} currents were blocked with 100 μM Cd^{2+} (data not shown), we did not find an indication that hyperpolarization affects transmitter release induced by Ca^{2+} uncaging.

We also show that the timing of phasic transmitter release is not completely invariant to changes in release probability brought about by varying the amount of Ca^{2+} influx (Figs. 4 and 5). We find that under voltage-clamp conditions, larger Ca^{2+} tail-currents evoke phasic transmitter release, with a shorter time difference between the peak of the Ca^{2+} currents, and the peak of transmitter release (Fig. 4 *d* and *e*). Why was the dependence of the timing of transmitter release on changes in Ca^{2+}-influx (Fig. 4) not found in previous studies (4, 15–17)? In most of the previous work, transmitter release after presynaptic APs was studied, and the release probability was altered by changing the extracellular $[Ca^{2+}]$. However, it is has been shown at the calyx of Held that changes in extracellular $[Ca^{2+}]$ lead to pronounced changes in the presynaptic AP waveform, which are expected to compensate for the reduction in peak time difference (see figure 2*A* of ref. 35). Another difference is that, in many previous studies, latency histograms with time bins of >100

μs were used (4, 15, 16, 19), rendering the resolution of time differences of 200 μs or less (Fig. 4*e*) nearly impossible. We have used deconvolution of EPSC traces sampled at time intervals of 20 μs, which has allowed us to measure changes in the timing of transmitter release as low as 40 μs. On the other hand, differences between various types of synapses cannot be excluded at present. Note that for the experiments in Fig. 4, the amount of Ca^{2+} influx was modulated by varying the number of Ca^{2+} channels opened during the depolarizations. The finding of a power relation with exponent close to 4 between transmitter release and Ca^{2+} current (Fig. 4*c Inset*) indicates (9) that the local $[Ca^{2+}]_i$ signal for vesicle fusion arises from several overlapping Ca^{2+} channels, in agreement with previous studies at the calyx of Held (4, 10).

To quantitatively predict the observed reduction of peak time difference (Fig. 4*e*), we first estimated the local $[Ca^{2+}]_i$ for transmitter release, which is compatible with the intracellular Ca^{2+} sensitivity of transmitter release measured in Fig. 3. For this analysis (Fig. 5), we assumed that the time course of the local $[Ca^{2+}]_i$ closely matches that of the time course of the presynaptic Ca^{2+} tail-current (Fig. 4*a*, solid traces). This assumption is justified to some extent if the local $[Ca^{2+}]_i$ is created by the overlap of several nearby Ca^{2+} channels (4, 10) although one would expect a slightly slowed decay of the microdomain $[Ca^{2+}]_i$ signal with respect to the decay of the whole-cell Ca^{2+} current. Waveforms of local $[Ca^{2+}]_i$ identical to the waveforms of Ca^{2+} currents predicted transmitter release rates with time courses similar to the observed ones (Fig. 5*a*). Also, the finding of decreased peak time differences with increasing $[Ca^{2+}]_i$ were predicted correctly (Fig. 5*b*). However, the predicted *absolute* peak time differences were faster by $\approx$280 μs over the entire range of Ca^{2+} concentrations tested (Fig. 5*b*, compare broken and solid gray lines). Interestingly, a slightly different model of Ca^{2+} dependent activation of vesicle fusion, which assumes independent instead of cooperative Ca^{2+} binding, also predicts an unexplained delay of several hundred μs (10, 13). This unexplained delay might constitute part of the "minimal" synaptic delay that would persist even at very high Ca^{2+} concentrations and probably reflects kinetic steps downstream from the action of Ca^{2+} at the Ca^{2+} sensor for vesicle fusion.

We showed that membrane potential does not have a direct influence on transmitter release at a CNS synapse and that the time course of phasic transmitter release is not completely invariant to changes in release probability. These findings validate the view that Ca^{2+} determines the kinetics of transmitter release and that simple models of Ca^{2+}-dependent activation of vesicle fusion adequately describe the final steps of vesicle fusion control in a glutamatergic CNS synapse, without the need to postulate a direct effect of presynaptic membrane potential.

We thank Bob Zucker for comments on the manuscript. This work was supported by Deutsche Forschungsgemeinschaft Grants SFB-406 and Schn 451/4-1. R.S. is a Heisenberg fellow of the Deutsche Forschungsgemeinschaft.

1. Katz, B. & Miledi, R. (1965) *Proc. R. Soc. London Ser. B* **161,** 483–495.
2. Llinas, R., Steinberg, I. Z. & Walton, K. (1981) *Biophys. J.* **33,** 323–351.
3. Augustine, G. J., Charlton, M. P. & Smith, S. J. (1985) *J. Physiol.* **369,** 163–181.
4. Borst, J. G. & Sakmann, B. (1996) *Nature* **383,** 431–434.
5. Bischofberger, J., Geiger, J. R. & Jonas, P. (2002) *J. Neurosci.* **22,** 10593–10602.
6. Barrett, E. F. & Stevens, C. F. (1972) *J. Physiol.* **227,** 691–708.
7. Simon, S. M. & Llinas, R. R. (1985) *Biophys. J.* **48,** 485–498.
8. Yamada, W. M. & Zucker, R. S. (1992) *Biophys. J.* **61,** 671–682.
9. Augustine, G. J., Adler, E. M. & Charlton, M. P. (1991) *Ann. N.Y. Acad. Sci.* **635,** 365–381.
10. Meinrenken, C. J., Borst, J. G. & Sakmann, B. (2002) *J. Neurosci.* **22,** 1648–1667.
11. Schneggenburger, R. & Neher, E. (2000) *Nature* **406,** 889–893.
12. Chow, R. H., Klingauf, J. & Neher, E. (1994) *Proc. Natl. Acad. Sci. USA* **91,** 12765–12769.
13. Bollmann, J. H., Sakmann, B. & Borst, J. G. (2000) *Science* **289,** 953–957.
14. Felmy, F., Neher, E. & Schneggenburger, R. (2003) *Neuron* **37,** 801–811.
15. Datyner, N. B. & Gage, P. W. (1980) *J. Physiol.* **303,** 299–314.
16. Parnas, H., Dudel, J. & Parnas, I. (1986) *Pflügers Arch.* **406,** 121–130.
17. Van der Kloot, W. (1988) *J. Physiol.* **402,** 605–626.
18. Parnas, H., Valle-Lisboa, J. C. & Segel, L. A. (2002) *Proc. Natl. Acad. Sci. USA* **99,** 17149–17154.
19. Hochner, B., Parnas, H. & Parnas, I. (1989) *Nature* **342,** 433–435.
20. Zucker, R. S. & Haydon, P. G. (1988) *Nature* **335,** 360–362.
21. Mulkey, R. M. & Zucker, R. S. (1991) *Nature* **350,** 153–155.
22. Landò, L. & Zucker, R. S. (1994) *J. Neurophysiol.* **72,** 825–830.
23. Zhang, C. & Zhou, Z. (2002) *Nat. Neurosci.* **5,** 425–430.
24. Mochida, S., Yokoyama, C. T., Kim, D. K., Itoh, K. & Catterall, W. A. (1998) *Proc. Natl. Acad. Sci. USA* **95,** 14523–14528.
25. Linial, M., Ilouz, N. & Parnas, H. (1997) *J. Physiol.* **504,** 251–258.
26. Wu, L. G., Borst, J. G. & Sakmann, B. (1998) *Proc. Natl. Acad. Sci. USA* **95,** 4720–4725.
27. Iwasaki, S. & Takahashi, T. (1998) *J. Physiol.* **509,** 419–423.
28. Grynkiewicz, G., Poenie, M. & Tsien, R. Y. (1985) *J. Biol. Chem.* **260,** 3440–3450.
29. Neher, E. & Sakaba, T. (2001) *J. Neurosci.* **21,** 444–461.
30. Meyer, A. C., Neher, E. & Schneggenburger, R. (2001) *J. Neurosci.* **21,** 7889–7900.
31. Scheuss, V., Schneggenburger, R. & Neher, E. (2002) *J. Neurosci.* **22,** 728–739.
32. Gillis, K. D. (1995) in *Single-Channel Recording*, eds. Sakmann, B. & Neher, E. (Plenum, New York), 2nd Ed., pp. 155–198.
33. Parnas, I., Parnas, H. & Dudel, J. (1986) *Pflügers Arch.* **406,** 131–137.
34. Dudel, J. (1984) *Pflügers Arch.* **402,** 235–243.
35. Schneggenburger, R., Meyer, A. C. & Neher, E. (1999) *Neuron* **23,** 399–409.